Electronic Supplementary Material (ESI) for Dalton Transactions.
This journal is © The Royal Society of Chemistry 2022

Supporting Information

for

Synthesis, crystal polymorphism and spin crossover behavior of the adamantylboron-capped cobalt(II) hexachloroclathrochelate and its transformation into the $Co^{III}Co^{II}Co^{III}$-bis-macrobicyclic derivative

Alexander S. Belov,[a,b] Valentin V. Novikov,[b,c] Anna V. Vologzhanina,[b] Alexander A. Pavlov,[b,c] Artem S. Bogomyakov,[d] Yan V. Zubavichus,[e] Roman D. Svetogorov,[f] Genrikh .E. Zelinskii,[a,b] Yan Z. Voloshin [a,b]

[a] *Kurnakov Institute of General and Inorganic Chemistry of the Russian Academy of Sciences, 119991 Moscow, Russia*

[b] *Nesmeyanov Institute of the Organoelement Compounds of the Russian Academy of Sciences, 119334 Moscow, Russia*

[c] *National Research University Higher School of Economics, 101000 Moscow, Russia*

[d] *International Tomography Center, Siberian Branch of the Russian Academy of Sciences, 630090 Novosibirsk, Russia*

[e] *Synchrotron Radiation Facility SKIF, G.K. Boreskov Institute of Catalysis of the Siberian Branch of the Russian Academy of Sciences, 630559, Koltsovo, Russia*

[f] *National Research Center Kurchatov Institute, 123182 Moscow, Russia*

***IR spectrum of* 1**

IR spectrum of its fine-crystalline sample in KBr contains the C = N, N – O and B – O bond stretching vibrations characteristic of the tris-dioximate boron-capped clathrochelates [S1]. The characteristic ν(C = N) band in this spectrum is substantially (by approximately 30 cm^{-1}) shifted in a high-frequency range, as compared with that in the spectrum of its known [S2] iron(II)-encapsulating analog.

***Morphology of the crystal packing of* 1**

It was studied with the Mercury package [S3].

We used the BFDH morphology tool of Mercury package [S3] to visualize the predominant direction of a crystal growth in the case of a hexagonal polymorph of **1** (Fig. S1, **b** and **c**). Faces of a predominant growth of the crystals **1** are formed by apical adamantyl groups of the corresponding clathrochelate molecules (Fig. S1, **c**), while its small side faces contain the chlorine ribbed substituents in the chelate α-dioximate fragments of **1** (Fig. S1, **b**). Contrary, a growth of the above crystals along their big crystal faces, which are formed by hydrophobic adamantyl substituents, is more slow. In its benzene solution, a growth in this direction is hampered because a quasiaromatic clathrochelate framework of this macrobicyclic molecule and aromatic benzene solvent molecules compete for formation of the corresponding hydrophobic interactions. This resulted in a growth of the plate crystals of a hexagonal polymorph of **1** with their twinned components, which are slightly disoriented along the crystallographic axis *c*. Trying to hamper a formation of the sandwich-like crystal packing of its clathrochelate molecules, we used a fast evaporation of the dichloromethane solution of **1** giving the fine-crystalline sample of this complex. Then, it was studied using the powder XRD method which suggested the formation of a triclinic polymorph of **1**. Asymmetric unit of this polymorph contains one macrobicyclic molecule in its general position. Atomic coordinates for this molecule were refined using the restraints for all its covalent bond lengths and its bond angles, while no those were applied to the encapsulated

cobalt ion and to the torsion angles as well. The obtained model possesses the covalent bond lengths which are close to those for the clathrochelate molecule **1** in the single crystal of its hexagonal polymorph. Orientations of their apical carbocyclic adamantyl substituents against to a macrobicyclic cage framework are also very similar.

UV-vis spectra

Deconvoluted solution UV-Vis spectrum of **1** (Fig.S10, **a**) contains the metal-to-ligand charge transfer (MLCT) $Co^{2+}d \rightarrow L\pi*$ bands in the visible and near-UV ranges with maxima from approximatelly 22100 to 17500 cm^{-1} ($\varepsilon \sim 0.1 \div 1.7 \cdot 10^3$ $mol^{-1}L\ cm^{-1}$). These relatively intensive bands mask those of a low intensity assigned to the *d–d* transitions in the encapsulated Co^{2+} ion. MLCT bands for a given cobalt(II) complex are substantially less intensive, as compared with those in the spectrum of its iron(II)-encapsulating analog $[Fe(Cl_2Gm)_3(BAd)_2]$: the latter contains three intensive ($\varepsilon \sim 1.5 \div 10 \cdot 10^3$ $mol^{-1}L\ cm^{-1}$) bands assigned to the $Fe^{2+}d \rightarrow L\pi*$ transitions in the same spectral range. UV range of the spectrum of **1** also contains a series of the intensive ($\varepsilon \sim 2.5 - 13 \cdot 10^3$ $mol^{-1}L\ cm^{-1}$) bands with maxima from approximately 27300 to 38000 cm^{-1} assigned to the $\pi - \pi*$ transitions in highly π-conjugated α-dioximate ribbed fragments of a quasiaromatic polyazomethine macrobicyclic ligand.

Solution UV-vis spectrum of **2** (Fig.S10, **b**) is dramatically different from that of the aforementioned cobalt(II)-encapsulating precursor. In particular, like the spectra of the hexamine [S6], aromatic and aliphatic [S1] cobalt(III) clathrochelates, it contains the low-intensive (830 and 320 $mol^{-1}L\ cm^{-1}$) bands of the ${}^1A_{1g} \rightarrow {}^1T_{1g}$ and ${}^1A_{1g} \rightarrow {}^1T_{2g}$ characteristic *d–d* transitions of the encapsulated Co^{3+} ion with maxima at 21132 and 17231 cm^{-1}, respectively (Table S1).

Energies of *d–d* transitions low-spin Co^{3+} ion in its pseudo-octahedral complexes can be calculated [S7] as:

$$\nu_1 = E({}^1T_{1g} \leftarrow {}^1A_{1g}) = 10\,Dq - C \qquad (1)$$

$$\nu_2 = E({}^1T_{2g} \leftarrow {}^1A_{1g}) = 10\,Dq - C + 16B \qquad (2)$$

If $C = 4B$, the ligand field parameters can be obtained using the following Eqs.3 and 4:

$$Dq = (3\,\nu_1 + \nu_2)/40 \qquad (3)$$

$$B = (\nu_2 - \nu_1)/16 \quad (4)$$

As it can be seen from Table S1, the field strength of a given dodecochloro-bis-clathrochelate ligand is substantially lower than those of their monomacrobicyclic analogs with aromatic and aliphatic substituents in their α-dioximate fragments [S1]. This can be due to a substantial electron-withdrawing effect of twelve ribbed strong electron-withdrawing chlorine atoms decreasing a donor ability of oxime groups of six chelating dichloroglyoximate moieties of a given bis-caging ligand.

Formation of the $Co^{III}Co^{II}Co^{III}$-trinuclear bis-clathrochelates

Unusual dodecasulfide $Co^{III}Co^{II}Co^{III}$-trinuclear bis-clathrochelates have been characterized [S6, S4] using the single-crystal XRD method among the by-products of an attempted nucleophilic substitution of $Co(Cl_2Gm)_3(BR)_2$ (where R = C_6H_5, C_6F_5) with alkyl- and arylthiolate anions. Boron-capped tris-α-dioximate *d*-metal monoclathrochelates are known [S1, S8] to possess the low chemical reactivity (in particular, they are unprecedently chemically robust even in harsh acidic media and/or in the presence of strong oxidants) and, therefore, a detachment of their capping fragments is extremely complicated. Most probable pathway of a formation of the dodecasulfide $Co^{III}Co^{II}Co^{III}$-trinuclear bis-clathrochelates shown in Scheme S1 is proposed [S4]. The corresponding hexachloromacrobicyclic cobalt(II)-encapsulating precursor undergoes a partial reduction with a given *S*-nucleophilic thiolate ion as reductant, thus giving a cobalt(I) clathrochelate. Its cage framework is relatively unstable, as compared with that of a cobalt(II)-encapsulating precursor, because of a higher Shannon radius of Co^+ ion, as compared with that of Co^{2+} ion. Cavity size of the boron-capped tris-dioximate ligands is known [S1, S8] to be quite optimal for encapsulation of the LS Fe^{2+} and Co^{3+} ions (their radii are equal to 0.75 and 0.68 Å, respectively), and, in a lesser extent, for that of the LS and HS cobalt(II) cations (0.79 and 0.85 Å, respectively). On the other hand, a size of the HS Co^+ ion seems to be much less matched to that of this cavity. So, the chemical reduction $Co^{2+/+}$ favors a detachment of one of the two alkyl- or arylboron containing cross-linking fragments to give the corresponding monocapped intermediate. Thus formed semiclathrochelate can give the aforementioned dodecasulfide $Co^{III}Co^{II}Co^{III}$-bis-clathrochelates by the following three most probable pathways. First of them includes a nucleophilic substitution of this hexachlorosemiclathrochelate with thiolate ions, followed by oxidation of the encapsulated cobalt ion, and by cross-linking of two formed hexasulfide cobalt(III) semiclathrochelate species with Co^{2+} ion as a bifunctional Lewis acid. The latter cation forms in the corresponding reaction mixture as a by-product of the side complete destruction reaction of a

given cage framework. The second probable pathway is based on a cross-linking of two hexachlorosemiclathrochelate species with Co^{2+} ion, thus giving the reactive dodecachloro-bis-clathrochelate intermediate. It easily undergoes a following nucleophilic substitution and an oxidation of the encapsulated cobalt(II) ions as well. Moreover, all these reactions (*i.e.*, nucleophilic substitution, cross-linking, and oxidation of the encapsulated metal ion) may be the consecutive processes. On the other hand, Pathway 2 (Scheme S1) that is based on the formation of an admixture of the $Co^{II}Co^{II}Co^{II}$-trinuclear dodecachloro-bis-clathrochelate precursor has been excluded [S6, S4] basing on the results of the additional synthetic experiments. So, Pathway 1 (Scheme S1) is described to be a most probable for the formation of these $Co^{III}Co^{II}Co^{III}$-trinuclear dodecasulfide bis-clathrochelates.

Another, even more unexpected, bis-cage product of a prolonged crystallization of the thiopheneboron-cross-linked tris-dimethylglyoximate monoclathrochelate $CoDm_3(BThioph)_2$ (see SI, Scheme S2) from its chloroform – heptane solution is described [S9]. Because the boron-capped macrobicyclic derivatives of aliphatic and aromatic α-dioximes are unprecedently chemically robust, the formed $Co^{III}Co^{II}Co^{III}$-trinuclear dodecamethyl-bis-cage complex $[CoDm_3(BThioph)]_2Co$ could not be derived from a probable cobalt(I)-containing semiclathrochelate intermediate, like in the case of its aforementioned alkyl- and arylsulfide analogs, due to the specific oxidative conditions of the corresponding template synthetic procedure. Moreover, we were unable [S9] to obtain this trinuclear intracomplex using the template condensation on the cobalt(II) ion as a matrix: this direct reaction with an excess of $CoCl_2$ performed under aerobic conditions in the presence of triethylamine as an organic base afforded only the cobalt(II) monoclathrochelate $CoDm_3(BThioph)_2$; even no traces of the target trinuclear complex $[CoDm_3(BThioph)]_2Co$ have been detected [S9] among its products. Therefore, this hexakis-dimethylglyoximate $Co^{III}Co^{II}Co^{III}$-bis-clathrochelate was a product of side chemical transformations of the initial monoclathrochelate $CoDm_3(BThioph)_2$ resulted from its reactions with phosgene and radical species, formed by photoinduced oxidation of chloroform in a course of its slow

evaporation. The latter process proceeds under air atmosphere (*i.e.* in the presence of air oxygen) in a chloroform solution of $CoDm_3(BThioph)_2$ deposited for a long time under sunlight irradiation. Indeed, the results of the performed [S9] detailed photochemical studies on irradiation of this solution under various experimental conditions allowed to suggest that the most probable pathway to the bis-clathrochelate $[CoDm_3(BThioph)]_2Co$, shown in Scheme S2, is based on a photoinitiated oxidation of $CHCl_3$ with O_2. It includes this radical process leading to the reactive species ($COCl_2$, HCl and the radical products), which caused the corresponding opening, rearrangement and re-capping reactions of a macrobicyclic framework of the molecule $CoDm_3(BThioph)_2$ to give its bis-cage derivative $[CoDm_3(BThioph)]_2Co$.

Quantum chemical calculations

All quantum chemical calculations were done using the ORCA package, v. 5.0. [S10]. Molecular geometry from the single crystal XRD structure of **1** was used as a starting point for the corresponding geometry optimization with the hybrid B3LYP functional, [S11] with the scalar relativistic zeroorder regular approximation (ZORA) and Grimme's DFT-D3 dispersion correction [S12] and the scalar relativistically recontracted (SARC) [S13], a version of the def2-TZVP [S14] basis set. Extra tight thresholds for forces and displacements were used. The solvation effects were included into these calculations using the Conductor-like Polarizable Continuum Model, as implemented. The calculate geometry was used to compute the g-tensor and isotropic values of hyperfine interaction tensors. Contact shift was calculated by the following equation [S15]:

$$\delta_C = \frac{S(S+1)\mu_B}{3kTg_N\mu_N} \cdot g_{iso} \cdot A_{iso} \qquad \text{(S1)}$$

where A_{iso} is the isotropic hyperfine coupling constant, g_{iso} is the isotropic electronic g-value, g_N is the nuclear g-value, μ_B and μ_N are the Bohr and nuclear magnetons, respectively, kT is the thermal energy.

In order to calculate a magnetic susceptibility anisotropy value from spin Hamiltonian parameters the following Eq. S2 as used [S16]:

$$\chi_{ab} = \frac{N_A kT \ \partial^2 lnZ}{10 \ \partial B_a \partial B_b} \qquad \text{(S2)}$$

where *a* and *b* are *x*, *y*, *z*; B is the external magnetic field; Z is a partition function equal to $\sum_{i=1}^{N} e^{\frac{-E_i}{kT}}$.

Axial anisotropy of χ-tensor was calculated using the following Eq. S3:

$$\Delta\chi_{ax} = \chi_{zz} - \frac{\chi_{xx} + \chi_{yy}}{2} \qquad \text{(S3)}$$

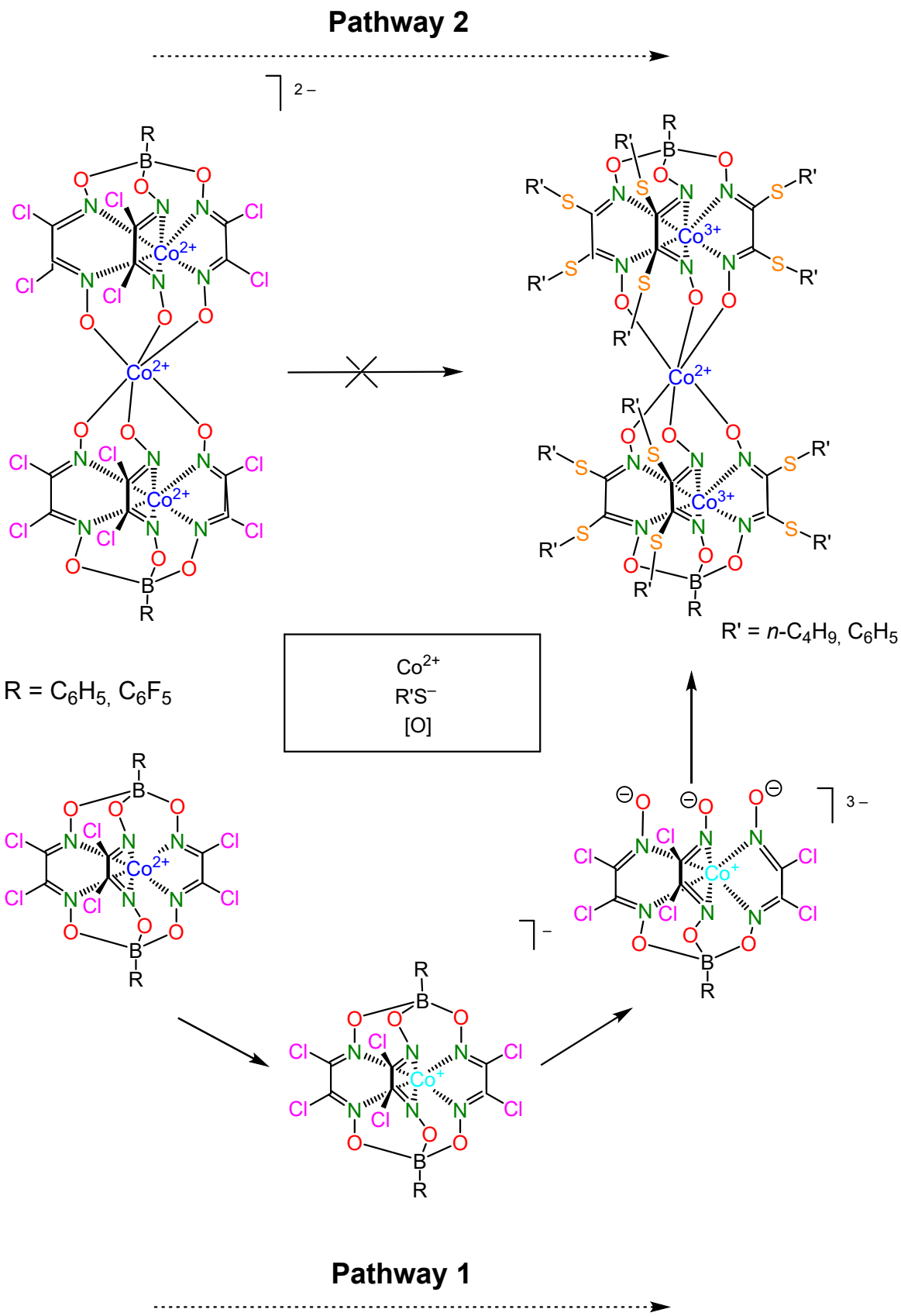

Scheme S1. Most probable pathway of a formation of the $Co^{III}Co^{II}Co^{III}$-trinuclear dodeca-alkyl- and arylsulfide bis-clathrochelates [S4].

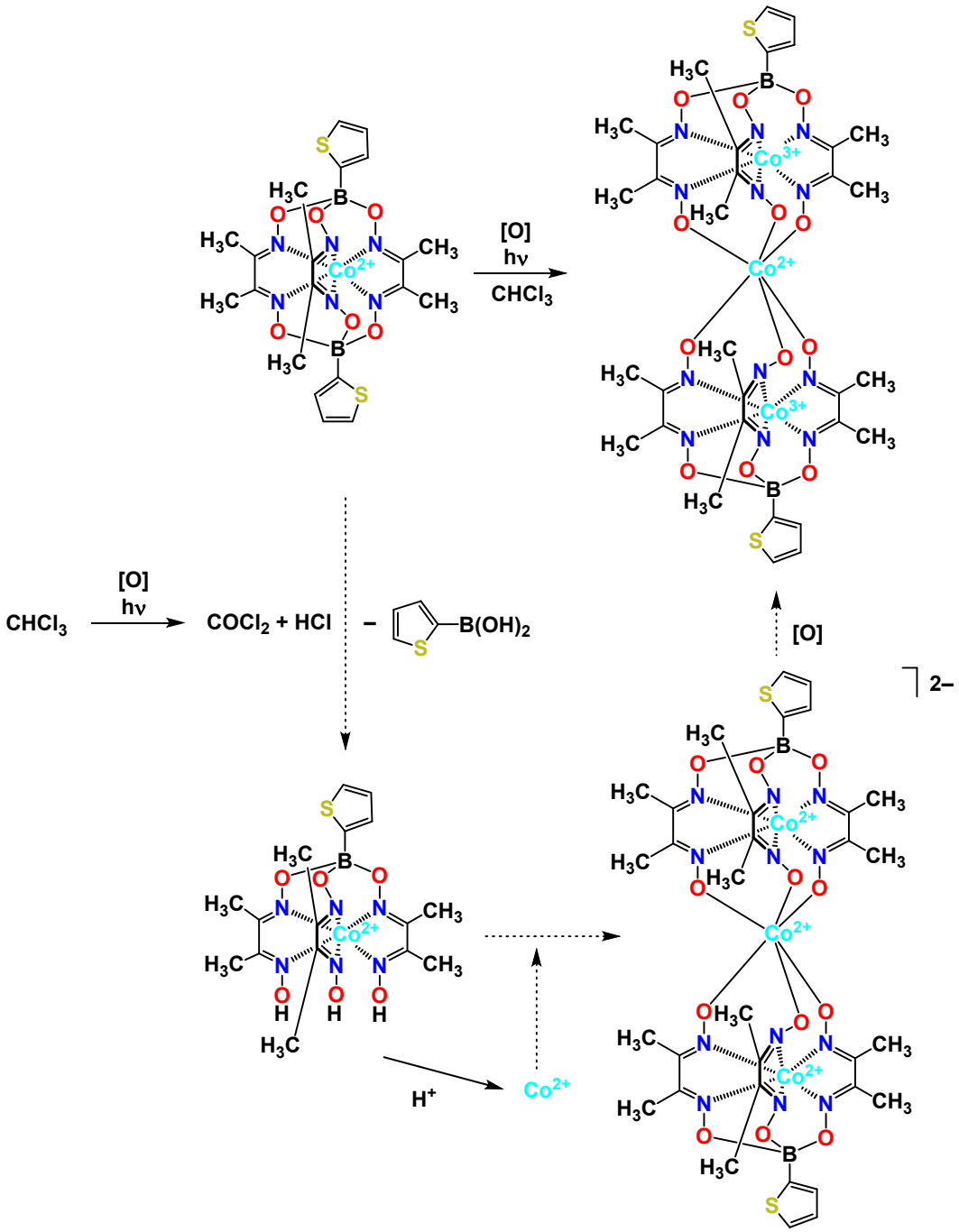

Scheme S2. Most probable pathway of a formation of the 2-thiopheneboron-capped $Co^{III}Co^{II}Co^{III}$-trinuclear dodecamethyl-bis-clathrochelate [S5].

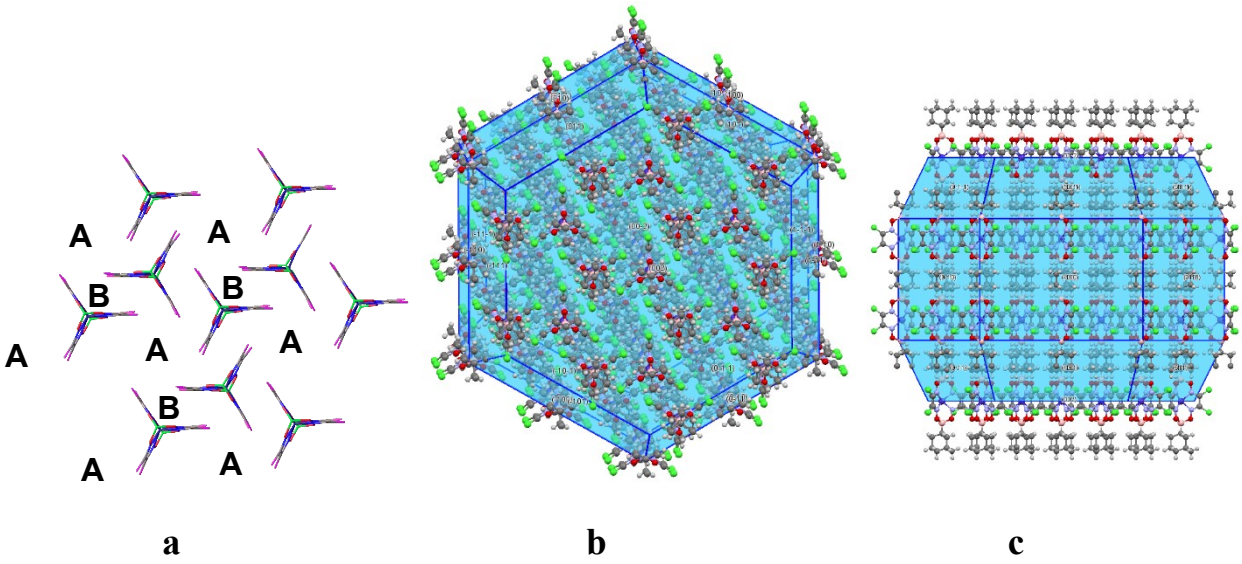

Figure S1. (**a**) Fragment of the crystal packing of a hexagonal polymorph of the clathrochelate **1** view along the crystallographic axis *c;* carbon and hydrogen atoms of its molecule are omitted for clarity), and the morphology of its crystal shape {views along the axes *c* (**b**) and *a* (**c**)}.

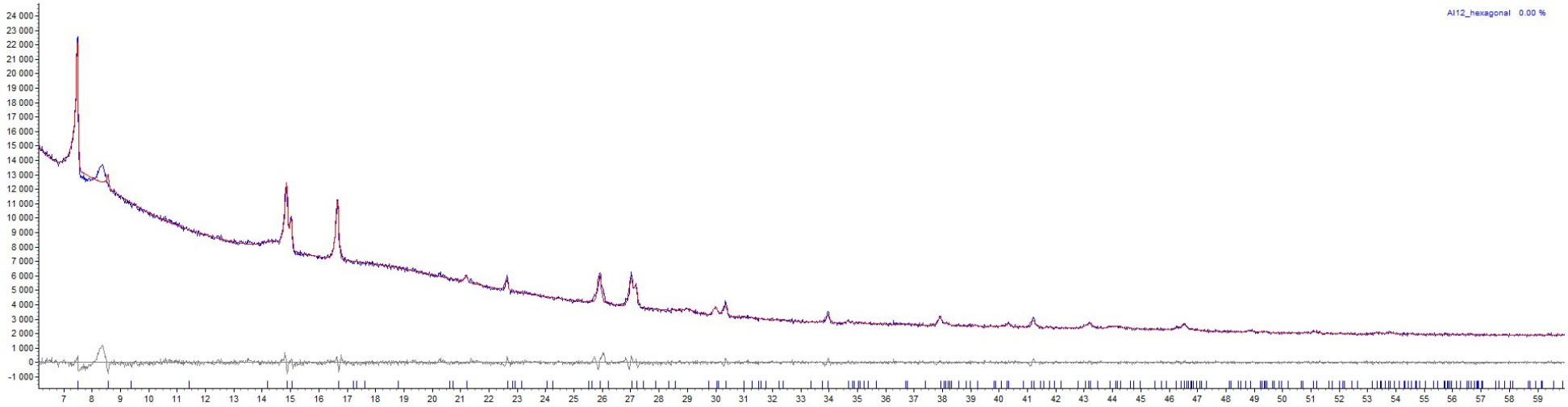

Figure S2. Experimental (blue) and theoretical (red) powder XRD pattern and their difference curve (gray) for the sample of a hexagonal polymorph of **1**, which was obtained by its recrystallization from the corresponding benzene solution (Rbragg / Rwp = 0.140 / 2.197).

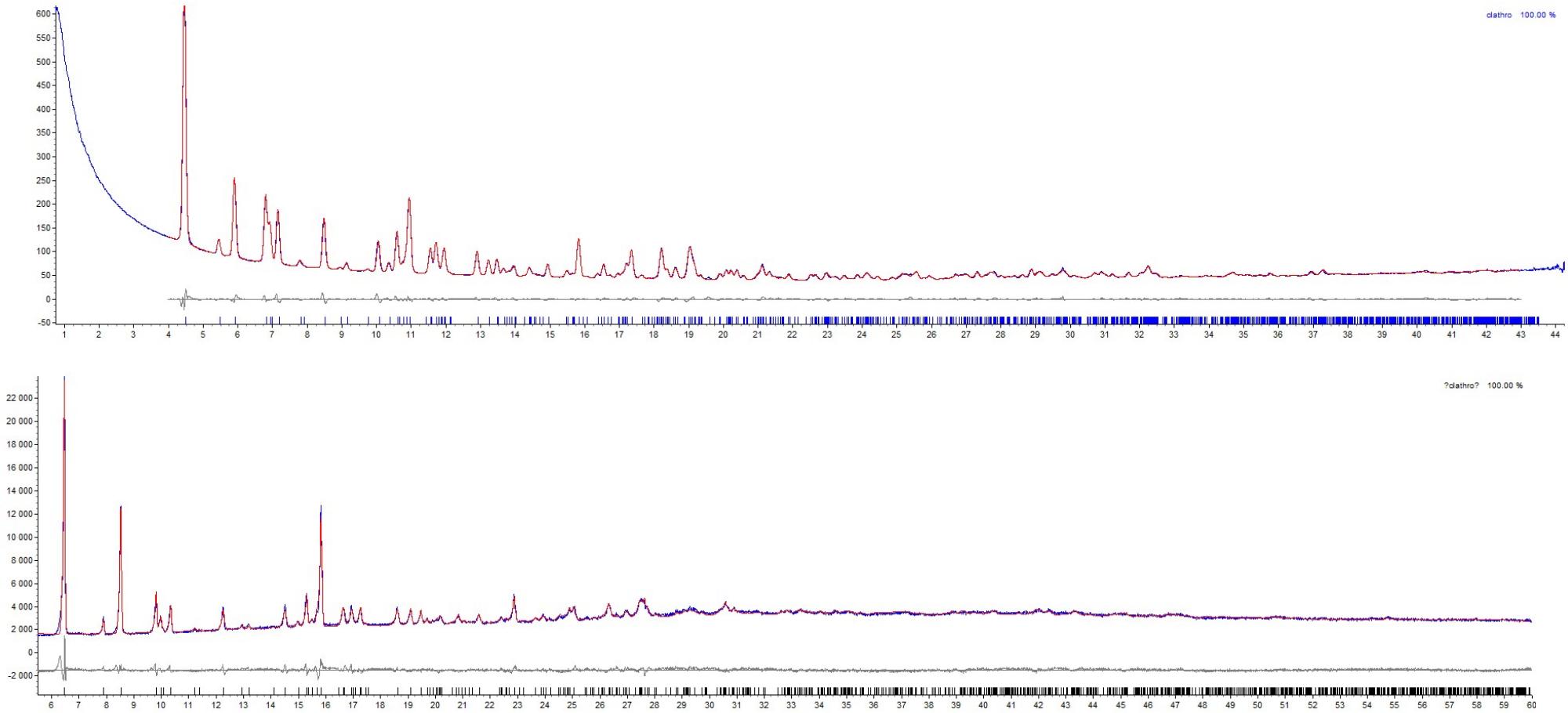

Figure S3. Experimental (blue) and theoretical (red) powder XRD pattern and their difference curve (gray) for the sample of a triclinic polymorph of **1**, which was obtained by a fast recrystallization from its CH_2Cl_2 solution. Top: as obtained at NRC "Kurchatov Institute" at 100 K using synchrotron radiation (Rbragg / Rwp = 0.43 / 2.01); bottom: as obtained with Bruker D8 Advance diffractometer at r.t. and CuKα radiation (Rbragg / Rwp = 1.388 / 3.811).

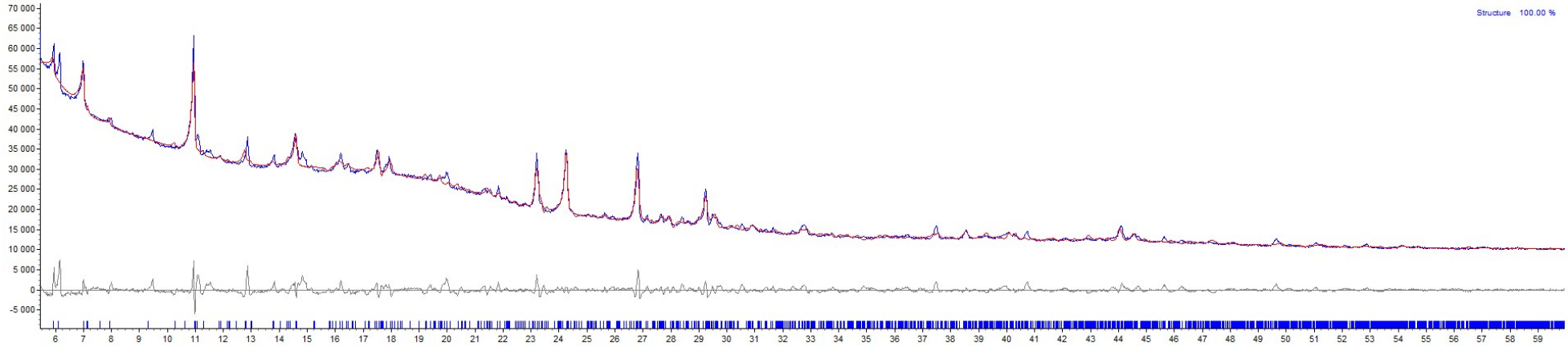

Figure S4. Experimental (blue) and theoretical (red) powder XRD pattern and their difference curve (gray) for the product of a prolonged crystallization of **1** from its dichloromethane solution deposited in air atmosphere on sunlight irradiation. It contains mainly the $Co^{III}Co^{II}Co^{III}$-trinuclear bis-clathrochelate **2** (Rbragg / Rwp = 1.554 / 3.009).

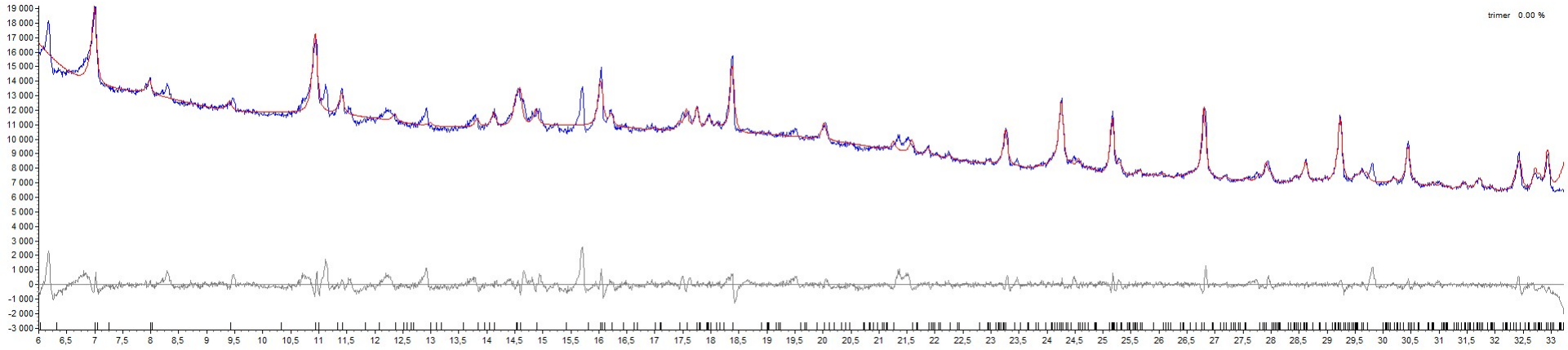

Figure S5. Experimental (blue) and theoretical (red) powder XRD pattern and their difference curve (gray) for the product of recrystallization of **1** from its dichloromethane solution. It contains mainly the $Co^{III}Co^{II}Co^{III}$-trinuclear bis-clathrochelate **2**.

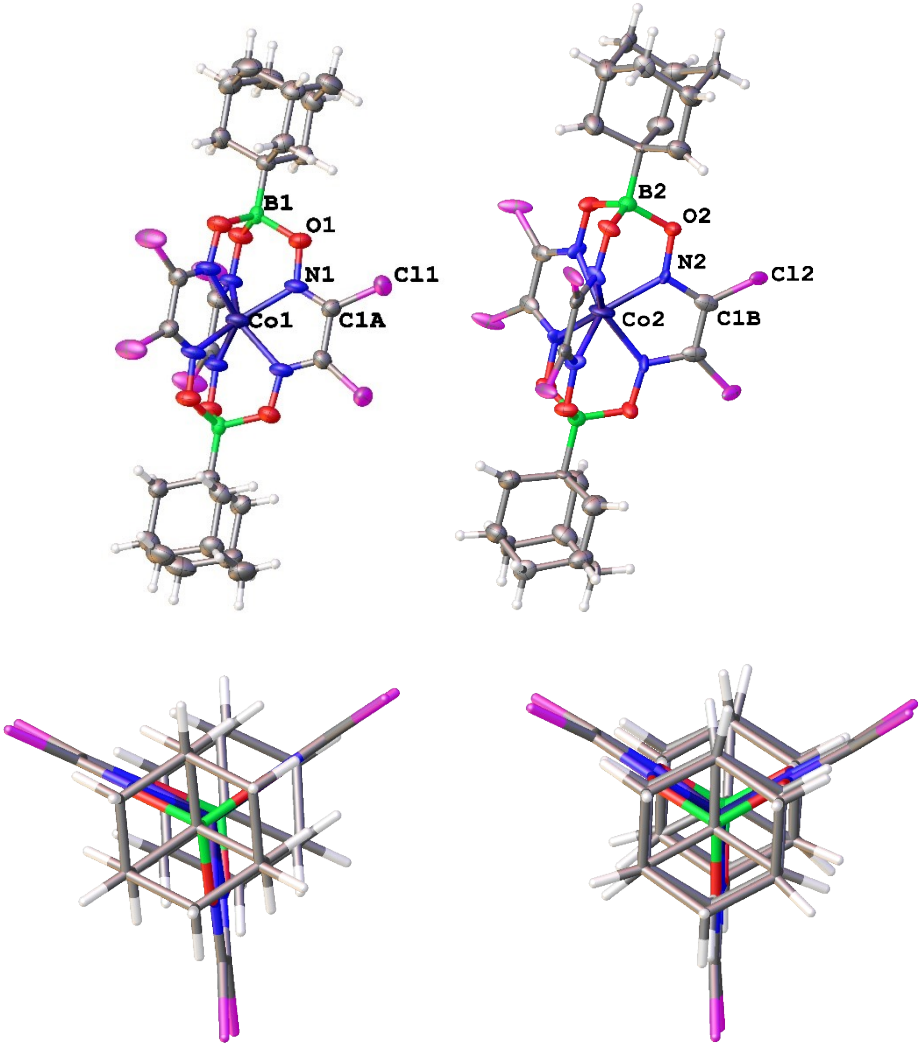

Figure S6. Side (on top) and top (along the molecular B...Fe...B C_3-pseudoaxis, on bottom) views of two independent clathrochelate molecules of **1** in representation of their atoms with thermal ellipsoids (p = 50%).

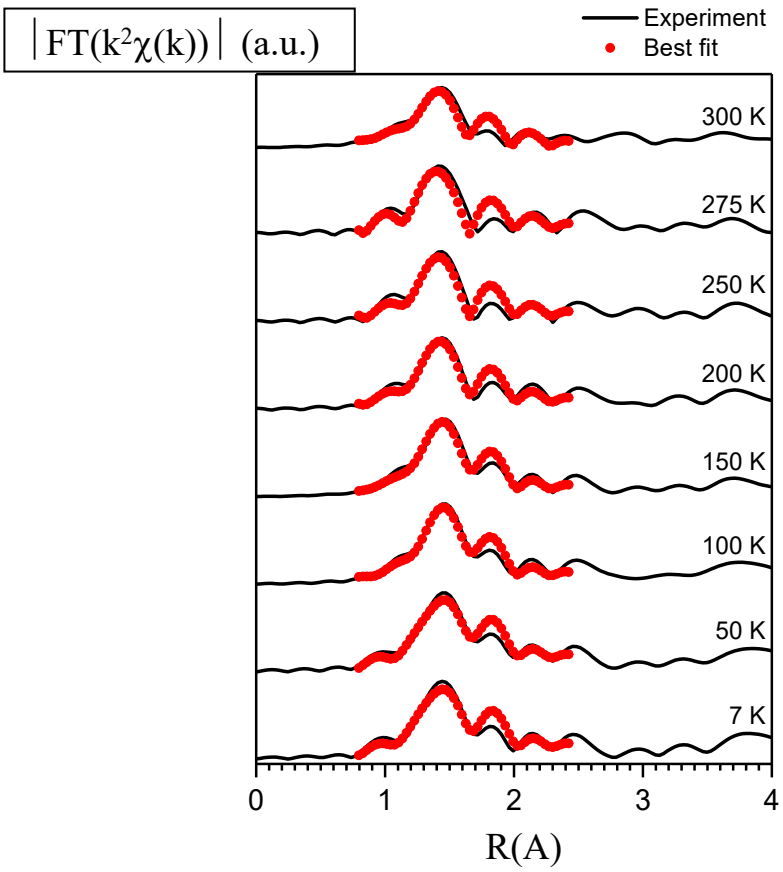

Figure S7. Refinement of EXAFS data for the fine-crystalline sample of a hexagonal polymorph of **1** in the R-space.

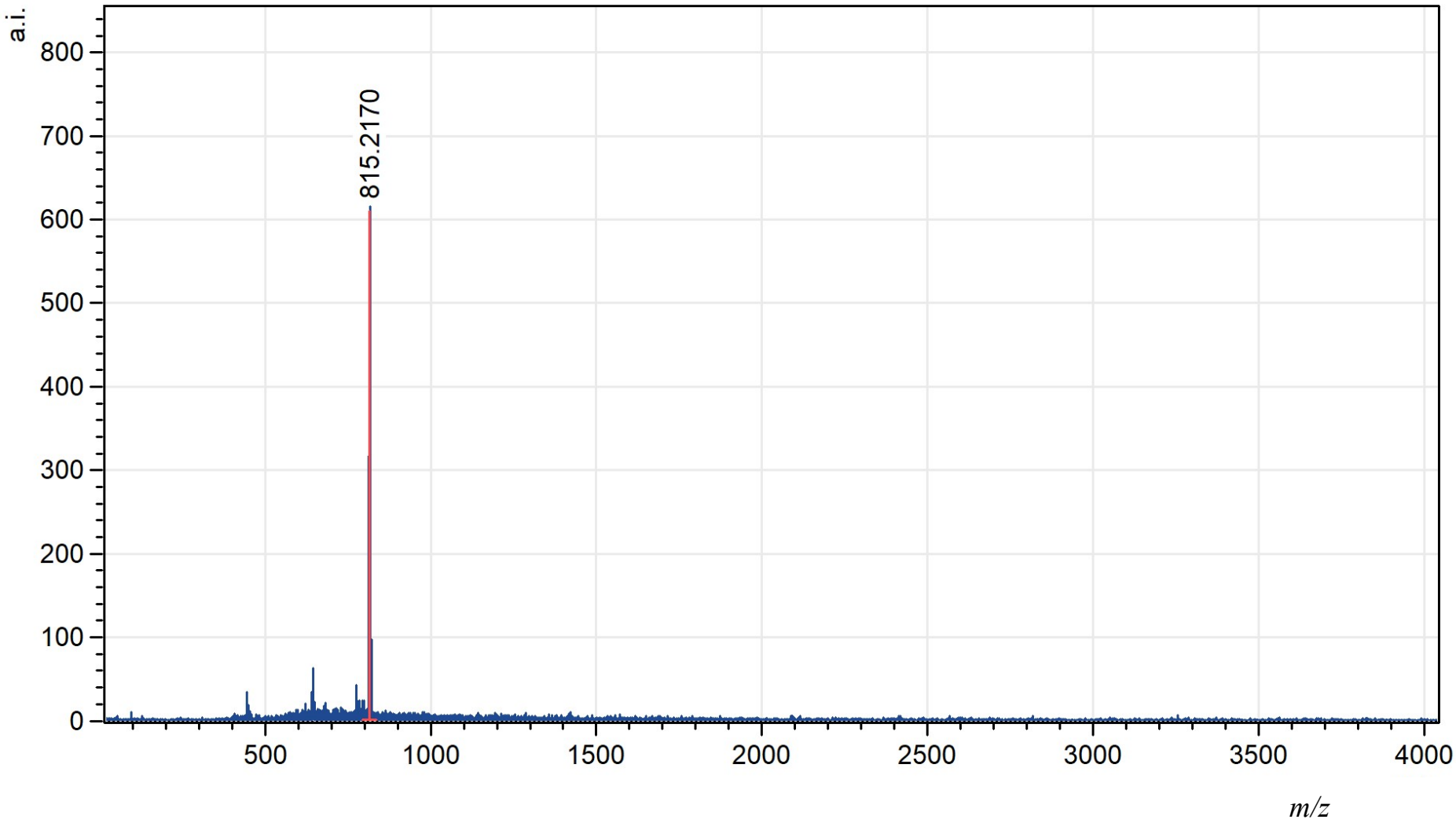

Figure S8. MALDI-TOF mass spectrum of the complex **1** in its positive range.

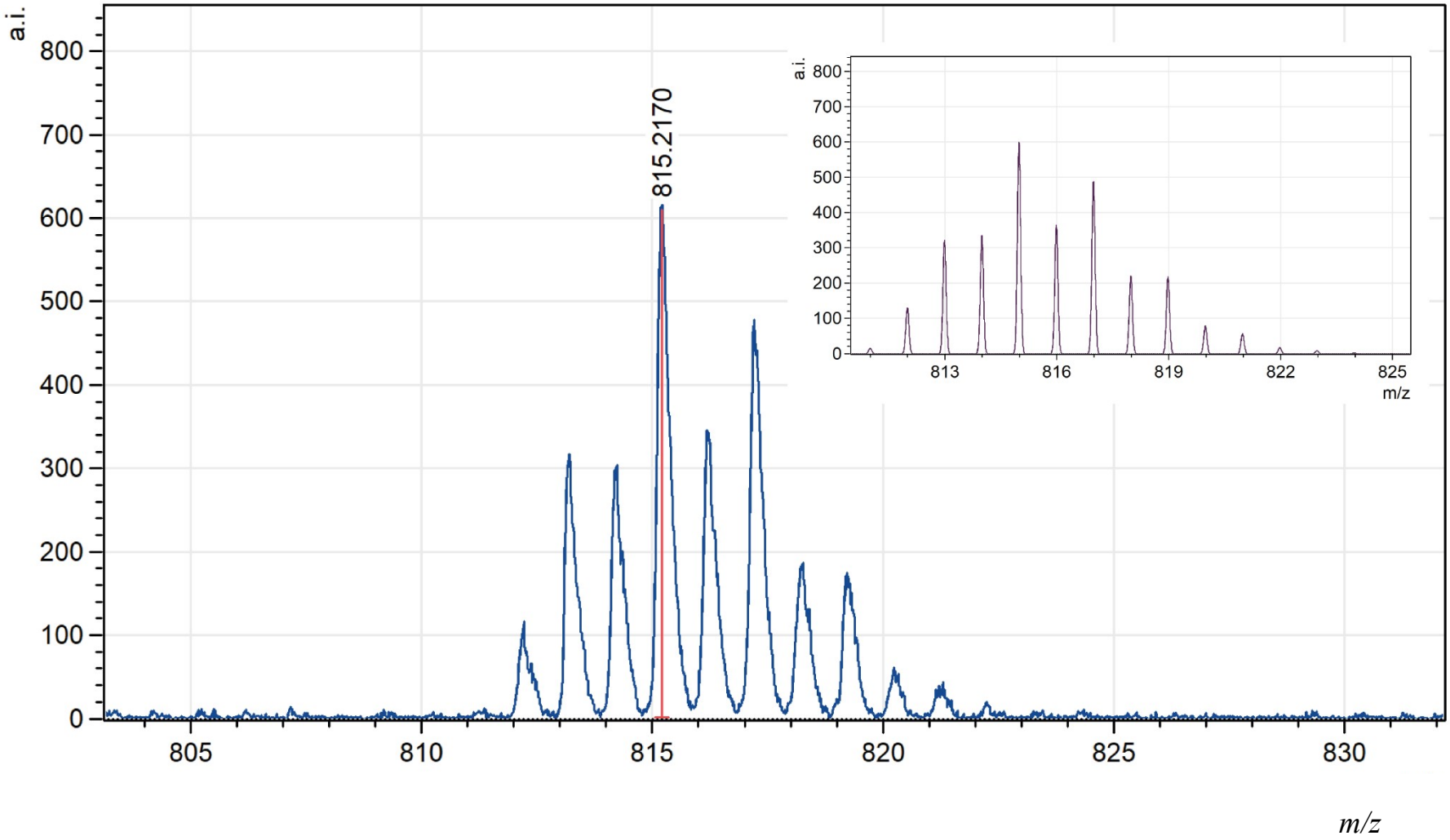

Figure S9. Fragment of the MALDI-TOF mass spectrum of the complex **1** in its positive range. Insert: the theoretically calculated isotopic distribution in its molecular ion.

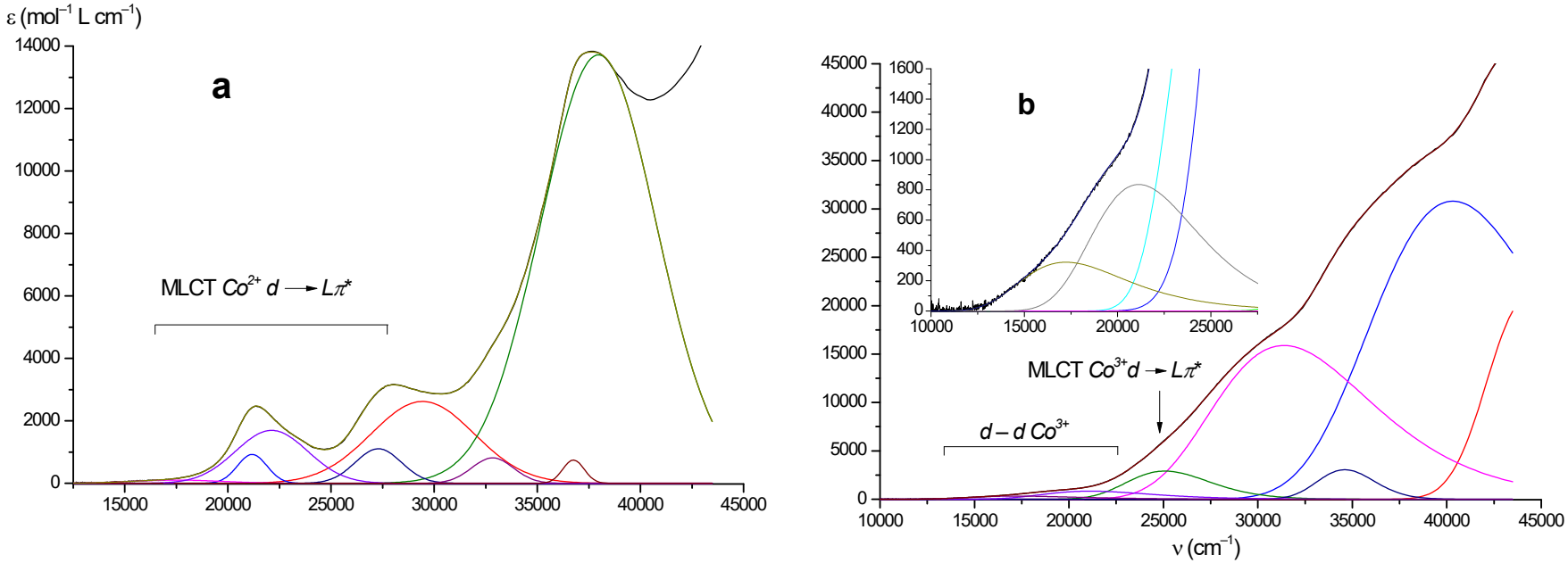

Figure S10. Deconvoluted UV-vis spectra of **1** (**a**) and **2** (**b**). Insert: Deconvolution of a fragment of the latter spectrum in the range of LS Co^{3+}-based *d*–*d* transitions.

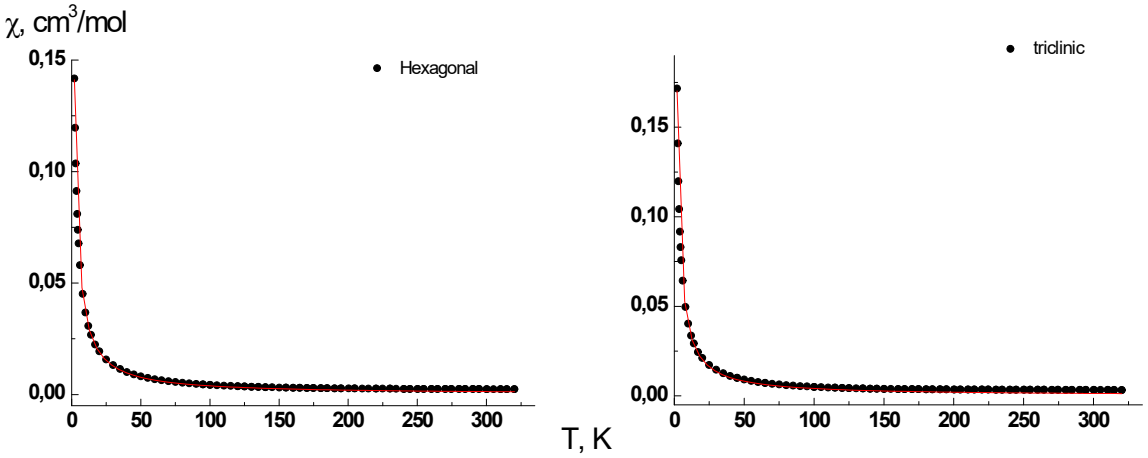

Figure S11. The experimental χ(T) dependencies for two polymorphs of **1** are shown. The Curie–Weiss law describes good the χ(T) dependencies with the following best fit values of C = 0.393±0.002 K·cm^3/mol and –0.78±0.02 K and C = 0.413±0.003 K·cm^3/mol and –0.42±0.03 K for its hexagonal and triclinic polymorphs, respectively.

Coordination polyhedra

Assignment of the coordination polyhedra was performed using the well-known approaches [S17 and S18]. In fact, the $Co^{II}N_6$-coordination polyhedra in both the polymorphs of **1** are formed by three rectangular edges and by two triangular edges (see below). This allowed to assign them to a trigonal-prismatic geometry [S17]. $Co^{III}N_6$- and $Co^{II}O_6$-coordination polyhedra in the bis-clathrochelate molecule **3** are formed by six triangular edges and, therefore, these may be assigned to the distorted octahedral geometry. However, basing on the approach [S18], only the $Co^{II}O_6$-coordination polyhedron of a cross-linking cobalt(II) ion can be described as an octahedron (due to the suitable value of the corresponding distorting angle φ between its opposite O_3-bases and the suitable values of the angels O–Co–O as well). Contrary, in the case of the $Co^{III}N_6$-coordination polyhedra of **3**, the corresponding distortion angles φ are close to 37°. This value is far from that for an ideal octahedral geometry with φ = 60°. Therefore, a rotational–translational distortion of this O_h geometry is observed and, thus, the can not be described as octahedra. Indeed, the $Co^{III}N_6$-coordination polyhedra in the molecule **3** undergo both a rotation of their N_3-basses along its molecular C_3-pseudoaxis and a contraction along this axis as well. Therefore, their geometry can be described as intermediate between a TP and a TAP (Figure S12).

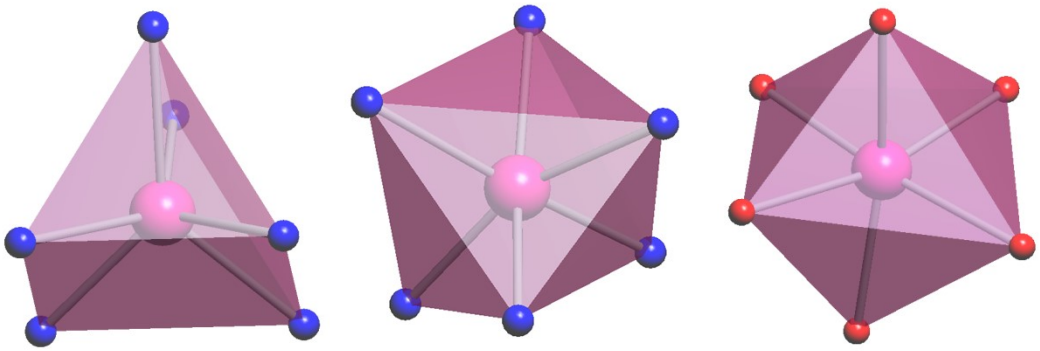

A **B** **C**

Figure S12. Trigonal-prismatic (**A**), intermediate trigonal-prismatic – trigonal-antiprismatic ("metaprismatic" in the terms of [S18]) (**B**) and octahedral (**C**) coordination polyhedra.

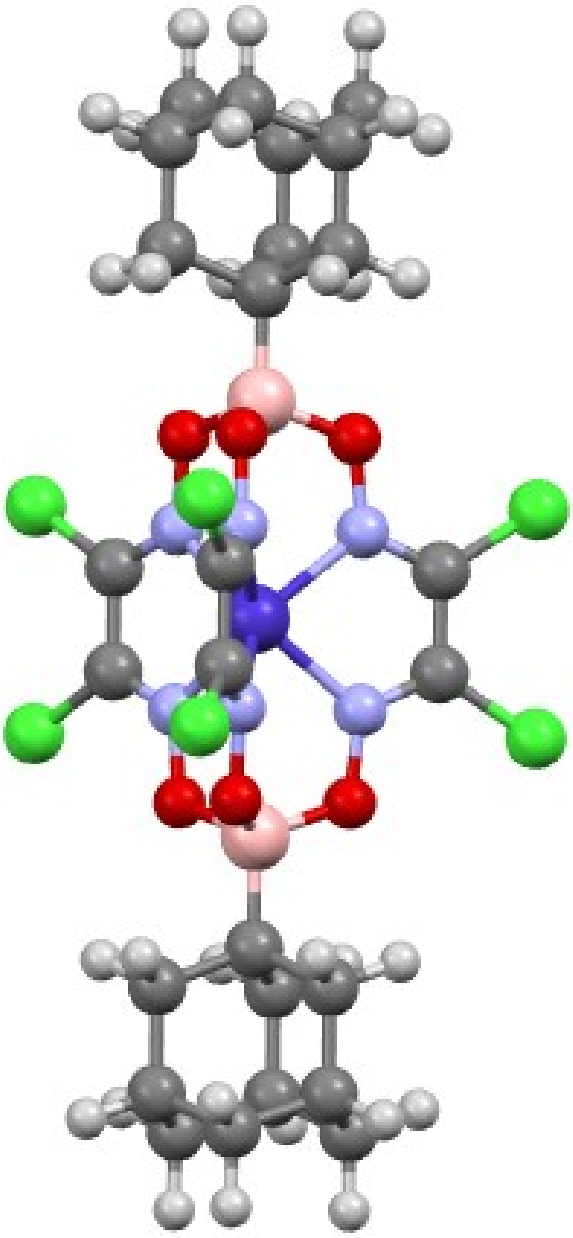

Figure S13. The optimized quantum-chemically calculated molecular structure of **1**.

Table S1. UV-vis spectral and crystal field parameters (cm^{-1}) for the cobalt(III) mono- and bis-clathrochelates

Complex	ν_2	ν_1	*Dq*	*B*
$[Co((n\text{-}C_4H_9NH)_2Gm)_3(BC_6H_5)_2](ClO_4)$ [S6]	19 610	17 010	1770	160
$[Co((n\text{-}C_4H_9NH)_2Gm)_3(BF)_2](ClO_4)$ [S6]	18 730	16 690	1720	130
$[Co((tert\text{-}C_4H_9NH)_2Gm)_3(BC_6H_5)_2](ClO_4)$ [S6]	19 960	16 840	1760	200
$[Co((C_6H_{11}NH)_2Gm)_3(BC_6H_5)_2](ClO_4)$ [S6]	20 080	17 540	1820	160
$[CoNx_3(BF)_2](BF_4)$ [S1]	29 600	19 800	2240	600
$[CoDm_3(BF)_2](BF_4)$ [S1]	30 200	19 800	2250	600
$[CoBd_3(BF)_2](BF_4)$ [S1]	27 300	21 700	2300	420
$H[CoDm_3(SnCl_3)_2]$ [S1]	26 300	21 800	2290	280
$H[CoNx_3(SnCl_3)_2]$ [S1]	26 500	22 300	2330	245
$H[CoNx_3(SnBr_3)_2]$ [S1]	25 200	20 900	2200	270
$(Co((n\text{-}C_4H_9S)_2Gm)_3(BC_6H_5))_2Co$ [S6]	22 120	21 280	2150	50
2	21 140	17 240	1820	245

Table S2. Crystallographic data and structure refinement details for hexagonal polymorph of **1** and its bis-clathrochelate derivative **2**

Compound	**1**	**2**·CH_2Cl_2·H_2Cl_2Gm
Empirical formula	$C_{26}H_{30}N_6O_6Cl_6B_2Co$	$C_{35}H_{35}B_2Cl_{17}Co_3N_{13}O_{13}$
Formula weight	815.81	1646.82
Crystal system	Hexagonal	Triclinic
Space group	$P\ \bar{6}\ 2\ c$	P –1
a (Å)	11.6072(19)	14.7689(5)
b (Å)	11.6072(19)	15.6801(6)
c (Å)	23.465(6)	16.1960(6)
α (deg)	90	91.230(2)
β (deg)	90	112.283(2)
γ (deg)	120	113.717(2)
Volume (Å^3)	2737.8(11)	3109.7(2)
Z	3	2
ρ_{calc} (g/cm^3)	1.484	1.759
μ (mm^{-1})	0.956	13.489
F(000)	1245	1640
Refls. collected	22958	50413
R_{int}	0.110	0.173
Data / restraints / parameters	3417 / 0 / 135	11855 / 6 / 749
Goodness-of-fit on F^2	0.134	1.06
R_1 [I>=2σ (I)]	0.134	0.086
wR2 [all data]	0.271	0.250
Largest diff. peak/hole (e Å^{-3})	1.673 / –0.826	0.883 / –0.892

Table S3. EXAFS data on amount of the HS form of a hexagonal polymorph of **1** at different temperatures

T (K)	ΔE (eV)	σ^2 (Å^2)	ω_{HS} (%)	R_f (%)
300	6.4	0.0013	29	2.7
275	6.0	0.0004	24	2.8
250	5.6	0.0008	19	2.7
200	5.4	0.0009	14	2.3
150	5.3	0.0018	0	2.2
100	5.1	0.0016	0	2.3
50	4.7	0.0014	0	2.4
7	5.1	0.0017	0	2.6

Table S4. Quantum-chemically optimized atomic coordinates for the molecule **1**

#	**Label**	**X**	**Y**	**Z**
1	Co	11.385	0.644	8.779
2	O	12.680	-2.056	8.726
3	O	11.678	2.463	11.140
4	O	10.495	-1.923	7.533
5	O	9.481	2.614	9.975
6	O	12.556	-0.915	6.515
7	O	11.536	3.625	8.944
8	N	12.510	-0.945	9.452
9	N	12.014	1.269	10.637
10	N	10.089	-0.837	8.194
11	N	9.586	1.416	9.397
12	N	12.408	0.305	7.035
13	N	11.911	2.554	8.242
14	B	12.011	-2.065	7.368
15	B	10.808	3.329	10.257
16	C	13.048	-0.832	10.639
17	C	12.765	0.443	11.320
18	C	8.824	-0.586	8.400
19	C	8.536	0.699	9.094
20	C	12.828	1.375	6.413
21	C	12.538	2.662	7.100
22	C	12.321	-3.458	6.624
23	C	11.777	-4.657	7.456
24	H	12.241	-4.657	8.468
25	H	10.678	-4.547	7.606
26	C	12.076	-5.998	6.745
27	H	11.677	-6.838	7.359
28	C	13.603	-6.162	6.573
29	H	14.100	-6.178	7.571
30	H	13.832	-7.136	6.081
31	C	14.155	-4.993	5.726
32	H	15.257	-5.108	5.604
33	C	13.478	-5.002	4.336
34	H	13.704	-5.956	3.804
35	H	13.883	-4.174	3.709
36	C	11.951	-4.838	4.506
37	H	11.461	-4.840	3.505
38	C	11.652	-3.497	5.218
39	H	10.550	-3.362	5.318
40	H	12.026	-2.650	4.596
41	C	11.399	-6.006	5.355
42	H	11.590	-6.978	4.840
43	H	10.295	-5.909	5.468
44	C	13.855	-3.653	6.437
45	H	14.275	-2.809	5.842
46	H	14.365	-3.632	7.428
47	C	10.494	4.720	11.004
48	C	11.813	5.486	11.318

49	H	12.475	4.855	11.954
50	H	12.369	5.686	10.374
51	C	11.513	6.821	12.041
52	H	12.473	7.347	12.253
53	C	10.773	6.535	13.367
54	H	11.413	5.913	14.036
55	H	10.571	7.490	13.908
56	C	9.447	5.799	13.070
57	H	8.915	5.589	14.027
58	C	8.559	6.685	12.166
59	H	7.590	6.171	11.961
60	H	8.314	7.641	12.685
61	C	9.299	6.971	10.840
62	H	8.658	7.607	10.185
63	C	9.600	5.637	10.117
64	H	10.109	5.840	9.147
65	H	8.644	5.117	9.874
66	C	10.625	7.707	11.138
67	H	10.420	8.683	11.638
68	H	11.156	7.939	10.185
69	C	9.748	4.465	12.348
70	H	8.796	3.918	12.157
71	H	10.366	3.811	13.005
72	Cl	14.010	-2.055	11.382
73	Cl	13.391	0.786	12.890
74	Cl	7.544	-1.619	7.887
75	Cl	6.916	1.186	9.421
76	Cl	13.635	1.346	4.891
77	Cl	12.980	4.166	6.387

Table S5. Main geometrical parameters of the boron-capped cobalt(II) hexachloroclathrochelate molecules

Parameter	**1**			$Co(Cl_2Gm)_3(BF)_2$ [12a]		$Co(Cl_2Gm)_3(Bn\text{-}C_4H_9)_2$ [12a]	$Co(Cl_2Gm)_3(BThioph)_2$ [33]	$Co(Cl_2Gm)_3(Bn\text{-}C_{16}H_{33})_2$ [12c]	
	Hexagonal		Triclinic						
	Type A	Type B		benzene solvate	toluene solvate				
M	LS Co^{2+}	LS Co^{2+}	LS Co^{2+}	HS Co^{2+}	HS Co^{2+}	LS Co^{2+}	LS Co^{2+}	LS Co^{2+}	HS Co^{2+}
Co – N (Å)	1.983(11)	1.941(15)	1.95(4) - 2.06(6)	2.033(1)	2.031(1)	1.894(2)–2.052(2)	1.942(5)–2.068(5)	1.908(5)–2.031(5)	1.970(3)–2.015(3)
B – O (Å)	1.528(12)	1.49(2)	*av.* 1.50	1.507	1.507	*av.* 1.509	*av.* 1.514	*av.* 1.528	*av.* 1.515
N – O (Å)	1.342(11)	1.35(2)	*av.* 1.35	1.357	1.360	*av.* 1.354	*av.* 1.359	*av.* 1.363	*av.* 1.362
C=N (Å)	1.254(16)	1.40(3)	*av.* 1.29	1.281	1.276	*av.* 1.289	*av.* 1.283	*av.* 1.312	*av.* 1.283
C – C (Å)	1.52(2)	1.47(4)	*av.* 1.47	1.492	1.490	*av.* 1.458	*av.* 1.473	*av.* 1.459	*av.* 1.467
N=C – C=N (°)	0	0	*av.* 10	0	0	*av.* 4.0	*av.* 2.8	*av.* 1.6	*av.* 0.5
φ (°)	0	0	3	0	0	7.8	5.1	3.1	1.9
α (°)	77.2	79.8	78.0	77.4	77.2	77.8	80.0	78.4	78.2
h (Å)	2.48	2.49	2.51	2.54	2.53	2.49	2.50	2.51	2.51

Table S6. Main geometrical parameters for the $Co^{III}Co^{II}Co^{III}$-trinuclear bis-clathrochelate molecules

Parameter	**2**		$[CoDm_3(BThioph)]_2Co$ [32]		$[(Co(C_6F_5S)_2Gm)_3(Bn\text{-}C_4H_9)]_2Co$ [31a]		$[(Co(n\text{-}C_4H_9S)_2Gm)_3(BC_6H_6)]_2Co$ [12a]		$[(Co(C_6F_5S)_2Gm)_3(B\text{-}C_6F_5)]_2Co$ [31b]	
M	Co^{3+}	Co^{2+}	Co^{3+}	Co^{2+}	Co^{3+}	Co^{2+}	Co^{3+}	Co^{2+}	Co^{3+}	Co^{2+}
Co – N (Å)	1.881(7) – 1.934(7)		1.882(6) – 1.918(6)		1.904(4) – 1.911(4)		1.905(1) – 1.920(2)		1.905(4) – 1.926(4)	
Co – O (Å)		2.035(6) – 2.078(6)		2.044(5) – 2.063(5)		2.056(3) – 2.085(6)		2.047(1) – 2.103(1)		2.042(4) – 2.094(4)
B – O (Å)	*av.* 1.52		*av.* 1.50		*av.* 1.513		*av.* 1.507		*av.* 1.505	
N – O (Å)	*av.* 1.370	*av.* 1.303	*av.* 1.396	*av.* 1.319	*av.* 1.374	*av.* 1.306	*av.* 1.380	*av.* 1.304	*av.* 1.374	*av.* 1.306
C=N (Å)	*av.* 1.30		*av.* 1.30		*av.* 1.300		*av.* 1.300		*av.* 1.300	
C – C (Å)	*av.* 1.45		*av.* 1.46		*av.* 1.454		*av.* 1.467		*av.* 1.451	
φ (°)	38.1	44.9	38.1	54.6	40.3	60.0	40.2	60	39.3	60.2
α (°)	40.9		40.1		40.9		40.7		40.7	
h (Å)	2.26 – 2.28	2.36	2.24	2.35	2.26	2.36	2.26	2.44	2.27	2.40

Supporting Information References

S1. Voloshin, Y.Z.; Kostromina, N.A.; Krämer, R. *Clathrochelates: Synthesis, Structure and Properties*; Elsevier: Amsterdam, Netherlands, 2002.

S2. Voloshin, Y.Z.; Varzatskii, O.A.; Belov, A.S.; Lebedev, A.Yu.; Makarov, I.S.; Gurskii, M.E.; Antipin, M.Yu.; Starikova, Z.A.; Bubnov, Y.N. Cage iron(II) complexes with apical and ribbed adamantyl substituents: The creation of second (hydrophobic) shell of an encapsulated metal ion. *Inorg.Chim. Acta*. **2007**, *360*, 1543–1554.

S3. Macrae, C. F.; Bruno, I. J.; Chisholm, J. A.; Edgington, P. R.; McCabe, P.; Pidcock, E.; Rodriguez-Monge, L.; Taylor, R.; van de Streek J.; Wood, P. A. Mercury CSD 2.0 – new features for the visualization and investigation of crystal structures. *J. Appl. Cryst*. **2008**, *41*, 466–470.

S4. (a) Voloshin, Y.Z.; Belaya, I.G.; Belov, A.S.; Platonov, V.E.; Maksimov, A.M.; Vologzhanina, A.V.; Starikova, Z.A.; Dolganov, A.V.; Novikov, V.V.; Bubnov, Y.N. Formation of the second superhydrophobic shell around an encapsulated metal ion: synthesis, X-ray structure and electrochemical study of the clathrochelate and bis-clathrochelate iron(II) and cobalt(II, III) dioximates with ribbed perfluoroarylsulfide substituents. *Dalton Trans*. **2012**, *41*, 737–746; (b) Belov, A.S.; Zelinskii, G.E.; Varzatskii, O.A.; Belaya, I.G.; Vologzhanina, A.V.; Dolganov, A.V.; Novikov, V.V.; Voloshin, Y.Z. Molecular design of cage iron(II) and cobalt(II,III) complexes with a second fluorine-enriched superhydrophobic shell. *Dalton Trans*. **2015**, *44*, 3773–3784.

S5. Belov, A.S.; Vologzhanina, A.V.; Fedorov, Y.V.; Kuznetsov, E.V.; Voloshin, Y.Z. Unexpected transformation of mono- to bis-macrobicyclic dimethylglyoximate framework in a chloroform solution: photochemical, MALDI-TOF MS and X-ray diffraction studies. *Inorg. Chem. Commun*. **2013**, *35*, 242 – 246.

S6. Voloshin, Y. Z.; Varzatskii, O. A.; Novikov, V. V.; Strizhakova, N. G.; Vorontsov, I.I.; Vologzhanina, A. V.; Lyssenko, K. A.; Romanenko, G. V.; Ovcharenko V. I., Bubnov, Y. N. Tris-dioximate cobalt(I,II,III) clathrochelates:

stabilization of different oxidation and spin states of an encapsulated metal ion by ribbed functionalization. *Eur. J. Inorg. Chem*. **2010**, 5401–5415.

S7. Lever, A.B.P. *Inorganic Electronic Spectroscopy*; Amsterdam, Elsevier, 1984.

S8. Voloshin, Y.Z.; Belaya, I.G.; Krämer, R. *Cage Metal Complexes: Clathrochelates Revisited*, Springer, 2017

S9. Belov, A.S.; Vologzhanina, A.V.; Fedorov, Y.V.; Kuznetsov, E.V.; Voloshin, Y.Z. Unexpected transformation of mono- to bis-macrobicyclic dimethylglyoximate framework in a chloroform solution: photochemical, MALDI-TOF MS and X-ray diffraction studies. *Inorg. Chem. Commun*. 2013, **35**, 242 – 246

S10. Neese, F. Software update: the ORCA program system, version 4.0. *Wiley Interdisciplinary Reviews: Computational Molecular Science*. 2018, *8*, e1327.

S11. Lee, C.; Yang, W.; Parr, R.G. Development of the Colle-Salvetti correlation-energy formula into a functional of the electron density. *Physic. Rev. B*. 1988, **37**, 785–789.

S12. Grimme, S.; Antony, J.; Ehrlich, S.; Krieg, H. A consistent and accurate ab initio parametrization of density functional dispersion correction (DFT-D) for the 94 elements H-Pu. *J.Chem.Phys*. 2010, **132**, 154104.

S13. Aravena, D.; Neese, F.; Pantazis, D.A. Improved segmented all-electron relativistically contracted basis sets for the lanthanides. *J. Chem. Theory Comput.* 2016, **12**, 1148–1156.

S14. Weigend, F.; Ahlrichs, R. Balanced basis sets of split valence, triple zeta valence and quadruple zeta valence quality for H to Rn: design and assessment of accuracy. *Phys.Chem.Chem.Phys*. 2005, **7**, 3297–3305.

S15. Kaupp, M.; Bühl, M.; Malkin, V. G. Calculation of NMR and EPR parameters: theory and applications. *John Wiley & Sons*, 2006.

S16. Atanasov, M.; Ganyushin, D.; Pantazis, D.A.; Sivalingam, K.; Neese, F. Detailed Ab initio first-principles study of the magnetic anisotropy in a family of trigonal pyramidal iron(II) pyrrolide complexes. *Inorg. Chem*. 2011, **50**, 7460–7477.

S17. Kepert, D. L. *Inorganic Stereochemistry*, Springer Verlag, Heidelberg, 1982

S18. Alvarez, S.; Avnir, D.; Llunell, M.; Pinsky, M. Continuous symmetry maps and shape classification. The case of six-coordinated metal compounds. *New J. Chem*., 2002, **26**, 996–1009